Rapid Communications

Hard-sphere-like dynamics in highly concentrated alpha-crystallin suspensions

Preeti Vodnala, Nuwan Karunaratne, and Laurence Lurio*
Department of Physics, Northern Illinois University, DeKalb, Illinois 60115, USA

George M. Thurston
School of Physics and Astronomy, Rochester Institute of Technology, Rochester, New York 14623, USA

Michael Vega and Elizabeth Gaillard
Department of Chemistry and Biochemistry, Northern Illinois University, DeKalb, Illinois 60115, USA

Suresh Narayanan, Alec Sandy, Qingteng Zhang, and Eric M. Dufresne
X-ray Science Division, Argonne National Laboratory, Lemont, Illinois 60439, USA

Giuseppe Foffi
Laboratoire de Physique des Solides, Université Paris-Saclay, CNRS, Université Paris-Sud, UMR 8502, 91405 Orsay, France

Pawel Grybos, Piotr Kmon, Piotr Maj, and Robert Szczygiel
AGH University of Science and Technology, av. Mickiewicza 30, Krakow 30-059, Poland

(Received 19 October 2017; published 2 February 2018)

The dynamics of concentrated suspensions of the eye-lens protein alpha crystallin have been measured using x-ray photon correlation spectroscopy. Measurements were made at wave vectors corresponding to the first peak in the hard-sphere structure factor and volume fractions close to the critical volume fraction for the glass transition. Langevin dynamics simulations were also performed in parallel to the experiments. The intermediate scattering function $f(q,\tau)$ could be fit using a stretched exponential decay for both experiments and numerical simulations. The measured relaxation times show good agreement with simulations for polydisperse hard-sphere colloids.

DOI: 10.1103/PhysRevE.97.020601

Significant progress has been made in understanding the glass transition in simple colloidal fluids, both from the study of model systems, such as latex [1] or silica [2] spheres and from comparison with theoretical models and molecular dynamics simulations, in particular, for hard-sphere fluids [3,4]. An important question is, to what extent do idealized hard-sphere systems represent real-world colloids? A system of particular relevance to biology is a concentrated protein suspension. The effect of high protein concentration on molecular dynamics, which has come to be termed "molecular crowding," is also a topic of particular interest in biophysics since crowding modifies reaction rates within a cell [5]. In the cytoplasm of the eye lens the concentration of proteins, called crystallins, can approach 70% [6,7]. There are three major mammalian crystallins, denoted alpha, beta, and gamma, of which alpha is both the largest and comprises ∼60% of the protein content by weight in humans.

Here we examine the dynamics of highly concentrated suspensions of alpha crystallin using x-ray photon correlation spectroscopy (XPCS) [8,9], small-angle x-ray scattering (SAXS), and Langevin dynamics (LD) simulations. XPCS is the x-ray analog of dynamic light scattering (DLS), but due to the shorter wavelength, XPCS probes much smaller length scales. Parallel use of LD allows us to test our microscopic interpretation of the XPCS and facilitates comparisons with existing DLS and neutron spin echo (NSE) results.

While many proteins isolated from living organisms are monodisperse, previous studies [10] have found polydispersities near 20% for the multisubunit alpha crystallins. As monodisperse colloids can more easily crystallize, alpha crystallin's polydispersity could reflect evolutionary pressures to avoid crystallization and the consequent scattering of light within the eye lens. Polydisperse hard-sphere models yield excellent descriptions of the static structure factor of alpha-crystallin suspensions. Foffi *et al.* [10] examined the structure and the dynamics of alpha-crystallin suspensions as a function of protein volume fraction ϕ, combining viscometry, small-angle neutron scattering, and dynamic light scattering. They found that the viscosity of concentrated suspensions could be described by mode coupling theory and molecular dynamics (MD) simulations of polydisperse hard-sphere colloids in the vicinity of a hard-sphere glass transition. Using DLS they measured the intermediate scattering function (ISF), which provides a measure of the characteristic relaxation time, τ, for density fluctuations at length scale $1/q$. Here $q = 4\pi n \sin(\theta/2)/\lambda$ is the scattering wave vector with n the index of refraction, λ the wavelength, and θ the scattering angle. Their DLS measurements were limited to length scales $\sim 2\pi/q = 2.7 \times 10^2$ nm, approximately 15 times the alpha-crystallin diameter [10]. This complicated comparison with MD, which could not simulate such large length scales. Furthermore,

*Corresponding author: llurio@niu.edu

deviations from Fickian diffusion are expected to be strongest at wave vectors that probe the separation of protein neighbor centers [4,11]. These are accessible to XPCS, but not DLS.

Bucciarelli *et al.* probed alpha-crystallin dynamics at wave vectors comparable to the present experiments using NSE, and found good agreement between hard-sphere dynamics and the initial, fast β decay of the ISF [12]. These measurements could not access the long-time α decay of the ISF which reflects important aspects of the approach to the glass transition [4,13]. Here, in complementary fashion, XPCS probes the α decay, but not the β decay.

Alpha-crystallin suspensions were prepared by homogenizing the lens cortex of 1- to 2-week-old calf eye lenses and then isolating the alpha crystallins via size exclusion chromatography, as described previously [14]. Proteins were suspended in 0.1 molar sodium phosphate buffer, pH 7.1, that contained 20 mM dithiothreitol (DTT) as an antioxidant. Suspensions of varying concentration were prepared from a stock solution at 100 mg/ml assayed via ultraviolet absorbance [15] and concentrated via centrifugation. Mass fractions were determined from changes to the weight of the solution upon removal of solvent. More accurate volume fractions were obtained from fitting to the static structure factors using a polydisperse hard-sphere model. Suspensions with concentrations up to 401 mg/ml were prepared in this manner.

SAXS and XPCS measurements were performed at sector 8-ID-I of the Advanced Photon Source. Crystallin suspensions were filled into 1-mm-diameter glass capillaries via centrifugation, and scattering was measured in transmission through the capillaries. The 7.34 keV x-ray beam was focused vertically using a Be compound refractive lens to 5.24 μm (FWHM), in order to increase the signal-to-noise ratio for XPCS [16]. Slits fixed the horizontal beam size to 20 μm. The incident x-ray flux within the illuminated volume was 6×10^{10} photons/s. XPCS measurements were performed using a custom pixel array detector called UFXC32k with 256(vertical) $\times$ 128(horizontal) 75 μm $\times$ 75 μm pixels capable of a frame rate of 11 000 fps [17,18].

Since globular proteins are known to aggregate under radiation exposure [19], we studied the effect of radiation dose on dynamics and concluded that the total dose, in the presence of 20 mM DTT, must be kept below 10^4 Gy [20]. Consequently, samples were translated through the beam with a vertical velocity of 0.025 mm/s, chosen to keep the dose below this value. This sample motion limited the longest correlation times that could be measured to $\sim$0.2 s. XPCS measurement times were limited by the total available sample since the sample was used up as it was damaged by the beam. Typical measurements were of order 10 min of integrated exposure.

Figure 1 shows normalized small-angle scattering intensity, $I(q)$. As the concentration is increased, a peak develops at larger q due to the structure factor consequences of the protein-protein nearest-neighbor peak. Simultaneously, the intensity at small q decreases due to the reduction in the osmotic compressibility. In order to extract the volume fractions, the SAXS data were fit to a polydisperse hard-sphere model $I(q)$ given by Vrij [21], employing analytic integrals obtained by Griffith *et al.* [22]. Representative fits are shown in Fig. 1. The polydispersity needed to fit the data was 18.3 $\pm$ 1.3%. Two separate average sphere radii were used in the model; one for

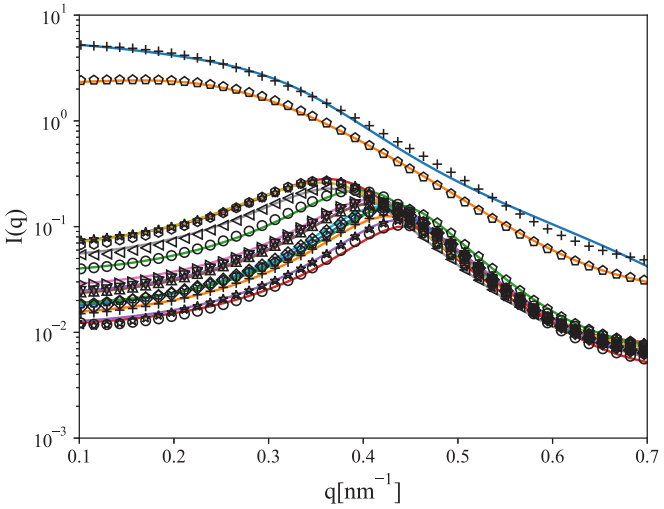

FIG. 1. Fits to SAXS from alpha-crystallin suspensions vs concentration. Data are normalized by their volume fractions. In order of largest to smallest intensity at low q, 44.5, 89, 250, 290, 300, 310, 320, 324, 325, 340, 347, 375, 379, 393, and 401 mg/ml.

the form factor of the proteins was found to be 6.3 $\pm$ 0.1 nm. A second describing the hard-sphere interaction radius came out to be 7.8 $\pm$ 0.3 nm. The polydispersity was taken to be the same for both radii.

The difference between the radius of the hard-sphere form factor and the radius of the hard-sphere structure factor implies that this is not an exact, but instead an effective hard-sphere system. Indeed, while it is convenient that the form factors of the spheres can be well fit using a polydisperse hard-sphere model, it is not expected that the exact shape of the proteins is spherical. Alpha crystallin is a multisubunit protein whose structure remains not known in detail and includes size, shape, and subunit-type heterogeneity [23–25], and it also includes intrinsically disordered segments that are believed to protrude into the solvent [26–28]. We take the radius obtained from the structure factor, not the form factor, as the appropriate radius. This radius is also compatible with what was found by Foffi *et al.* [10]. Similarly, we use volume fraction obtained from the hard-sphere structure factor fits as the appropriate volume fraction for the analysis of dynamics. Volume fractions were refined by using the results from the hard-sphere fits to calibrate the experimentally measured weight fractions. This resulted in a partial volume fraction of 1.47 $\pm$ 0.11 $\times$ 10^{-3} ml/mg, which differs significantly from that obtained by Foffi *et al.* of 1.7 $\times$ 10^{-3} ml/mg [10]. The relatively large ($\sim$10%) uncertainty in the absolute values of the volume fractions is due to the uncertainty in the partial volume fraction. Since all the samples were obtained from a single initial batch of crystallin via successive removal of solvent, the relative volume fractions of the samples are known to have significantly higher accuracy, comparable to the accuracy by which the change in mass of water could be measured ($\sim$0.1%).

Time correlation functions were calculated from the sequence of detected frames via

$$g_2(q,t) = \langle I(t,q)I(t'+t,q)\rangle_{t'}/\langle I\rangle^2. \quad (1)$$

g_2 can be related to the intermediate scattering function $f(q,t)$ via the Siegert relation $g_2(q,t) = 1 + \beta f(q,t)^2$. Here β is the

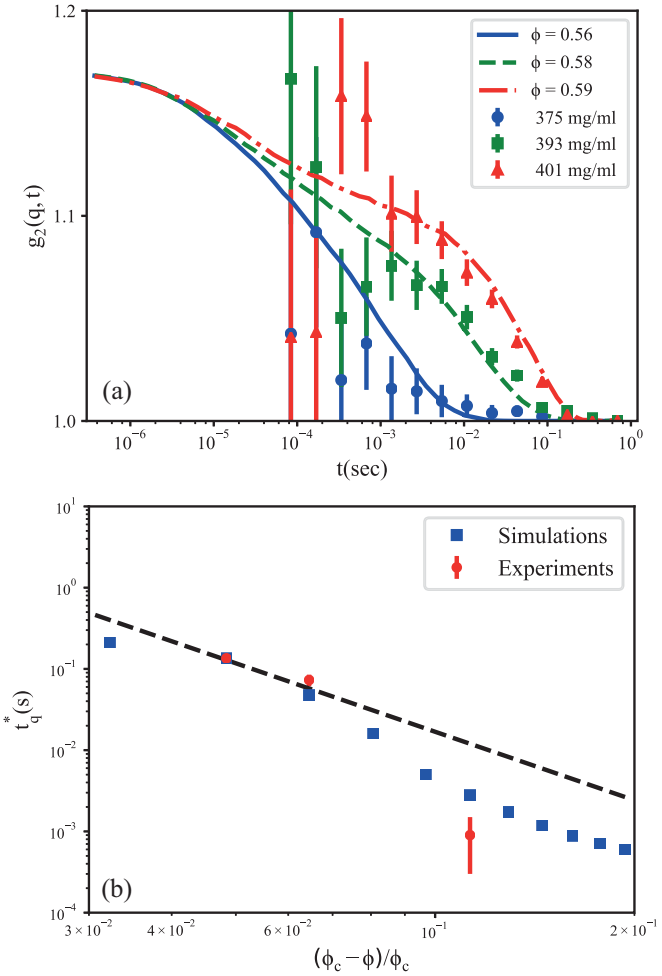

FIG. 2. Results of molecular dynamics simulations. (a) Simulated g_2 functions for 20% polydispersity at varying ϕ compared with XPCS. (b) t_q^* vs $\varepsilon = (\phi_c - \phi)/\phi_c$ for experiments and simulations. The dashed line is the theoretically expected scaling form close to the glass transition: $t_q^* \sim \varepsilon^{-\gamma}$ with $\gamma = 2.8$.

optical contrast factor. Correlation functions were measured at a wave vector q centered on the peak of the measured structure factor. The correlation functions were calculated within individual detector pixels and then averaged over all pixels within $\Delta q/q \approx 20\%$ comprising all the available camera area. Correlation functions for longer delay times were binned using a multi-tau algorithm [29]. $g_2(t)$ for protein suspensions with $\phi \leqslant 0.49$ were indistinguishable from unity, presumably due to dynamics faster than the time resolution of the camera. Figure 2(a) shows $g_2(t)$ for the three most concentrated suspensions with 375, 393, and 401 mg/ml corresponding to volume fractions of $0.55 \pm 0.04, 0.58 \pm 0.05, 0.59 \pm 0.05$ all in close vicinity of the theoretical hard-sphere critical volume fraction of $\phi = 0.579$.

The continuous translation of the sample through the beam will lead to a reduction in contrast with delay time. If r is the fractional overlap of the illuminated sample area between time t' and time $t' + t$, then the contrast will be reduced by a factor of r^2. If we assume a Gaussian beam profile characterized by a second moment σ, then this overlap factor can be computed

TABLE I. Relaxation times obtained from exponential fits to g_2 functions.

mg/ml	VF	t_q^*[s]
401	0.59	0.135 ± 0.014
393	0.58	0.073 ± 0.012
375	0.55	0.0009 ± 0.0006

analytically. The experimentally measured $g_2(t)$ is then given by

$$g_2(t) = 1 + \beta f(q,t)^2 e^{-(t/t_M)^2}. \quad (2)$$

Here $t_M = 2\sigma/v_z = 0.18$ s, with v_z the sample velocity. A derivation of Eq. (2) is given in the Supplemental Material [30]. We expect that only data at delay times longer than ~ 0.1 s will be significantly distorted by sample motion.

A measure of the α relaxation is the time, t_q^*, when $f(q,t_q^*) = 0.25$. We fit the intermediate scattering function to a stretched exponential of the form $f(q,t) = f_q e^{-(t/t_q^\alpha)^\beta}$ from which t_q^* could be extracted via $t_q^* = t_q^\alpha \ln(4f_q)^{1/\beta}$. The quality of the data was not high enough, however, to obtain the stretching exponent independent of t_q^* as there was too much correlation between β and t_q^α. Best-fit values for t_q^* are displayed in Table I.

We have also used LD to calculate $f(q,t)$ using an effective hard-sphere system with the same polydispersity as the experimental system, $p = 0.183$. Simulations were performed following the usual formulation with no hydrodynamic interactions:

$$m_i \ddot{\mathbf{r}}_\mathbf{i} = \sum_j \mathbf{F}_{ij} - \nu \dot{\mathbf{r}}_\mathbf{i} + \eta_i(t). \quad (3)$$

Here $\mathbf{F}_{ij}$ is the conservative force between the particles, ν is the friction coefficient, and η_i is a white-noise term whose prefactor is chosen to guarantee equilibrium following the fluctuation-dissipation theorem [31]. All the simulations were performed using LAMMPS [32]. Protein interactions were modeled by a power-law repulsive potential:

$$V(r_{ij}) = \epsilon \left(\frac{\sigma_{ij}}{r_{ij}} \right)^n. \quad (4)$$

Here $\sigma_{ij} = (\sigma_i + \sigma_j)/2$ is derived from the i-particle diameter σ_i, n is positive integer, and ϵ is an energy scale that has been set to unity. Particle sizes were sampled from a Schulz distribution with polydispersity p and mean $\langle \sigma_i \rangle = 1$. The masses of the particles were chosen to be proportional to their volumes, i.e., $m = m_0 \sigma^3$, where m_0 fixes the units of mass. The temperature was fixed to $k_B T = 1$. With this choice of parameters the reduced time units were derived from the thermal velocity $v_{\text{th}} = \sqrt{\frac{k_B T}{m_0}}$. This can be converted into real units by comparing the results to the experiments. It has been shown that if the parameter n is large enough, this model does a good job of reproducing the hard-sphere model [33,34]. In previous studies, it was claimed that $n = 36$ was sufficient to guarantee a good approximation for the steep hard-core repulsion. For the large polydispersity tested here, we found that $n = 72$ is a better choice even if this requires a quite

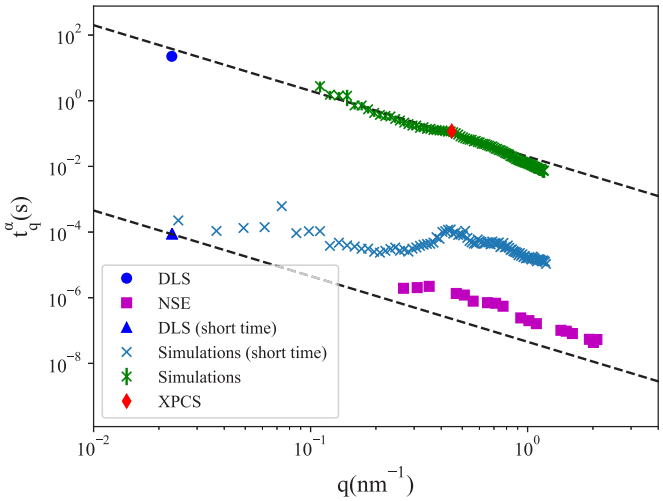

FIG. 3. Comparison of the q dependence of the simulations with the experimental data at $\phi = 0.59$ (see text). Upper (α relaxation) and lower (β relaxation) dashed lines are proportional to q^{-2}. The long-time DLS are taken from Ref. [10] (blue full circle) and the short-time DLS (blue full triangle) and NSE (magenta full square) are taken from Ref. [12].

short integration step for Eq. (3). With this choice, once the temperature is fixed to unity, the spheres behave as hard spheres of diameters σ_i and this permits a direct calculation of the packing fraction via $\phi = \frac{\pi}{6}\frac{\sum_i N_i \sigma_i^3}{L^3}$. Here N_i is the number of particles of the i species and L is the size of the simulation box. For all the simulations presented here, we used $N = 5000$. The particles were placed in a cubic box having periodic boundary conditions. At short times, Eq. (3) guarantees ballistic motion but after a relaxation time $\tau_L = m/\nu$ the diffusive regime is reached. Here, we have chosen $\tau_L = 0.01$ which guarantees that the inertial effects are present only at short time.

We scaled the arbitrary time units from the simulation to match the highest experimentally measured relaxation time obtained at a concentration of $\phi = 0.59$. The theoretically calculated relaxation times t_q^* are then compared with the remaining two experimentally measured data points in Fig. 2(b). Both simulation and experimental data are plotted using reduced volume fraction assuming $\phi_c = 0.62$ obtained from the simulations. The figure also shows the expected scaling law close to the glass transition of $t_q^* \sim [(\phi_c - \phi)/\phi_c]^{-\gamma}$ with exponent $\gamma = 2.8$ predicted by mode coupling theory [13]. A comparison of the experimental and numerical time correlation functions $g_2(t)$ is displayed in Fig. 2(a). Our model does a reasonable job of describing both the shape of the intermediate scattering function and the volume fraction dependence of the relaxation times.

The q dependence of the LD α-relaxation time t_q^α is presented in Fig. 3. The XPCS data are also plotted, with t_q^* converted to t_q^α using the same stretching exponent as obtained from the fits to the LD ISF. Since the simulations could not be extended all the way to low enough q to overlap with previously measured DLS data [10], a power-law extrapolation of the simulation data was performed. A power law of q^{-2} was chosen based on the shape of the scaling of the LD data. This extrapolation shows that the scaling of the LD time units using the XPCS data also yields reasonable agreement for the time scale of the DLS data.

To obtain a more complete picture of the system we must combine results from a variety of techniques. Such a comparison is done in Fig. 3 which displays DLS [10], NSE [12], and XPCS measurements of alpha-crystallin dynamics along with our LD simulations. It can be seen that the beta relaxation rate of the correlation function from NSE is around four times slower than for Fickian diffusion, shown as the lower dashed line. This deviation is consistent with hydrodynamic effects and de Gennes narrowing as discussed by Bucciarelli *et al.* [12]. The alpha relaxation measured using both DLS and XPCS is of order 10^5 times slower than the β relaxation time found by NSE. We studied whether LD could also be used to interpolate between the NSE and XPCS measurements by comparing the β and α relaxation rates. The short-time limit of the LD is also shown in Fig. 3 and does not agree with the NSE data.

The main reason for the disagreement between the NSE and the short-time LD simulations is to be ascribed to the small value of the friction coefficient, ν, chosen in Eq. (3). This choice limits the computation time, and this is expected to decrease the gap between the α and β relaxations. This is a limiting factor, particularly in glassy systems where the density relaxation can be observed at very long times, which affects all such coarse-grained simulations [35]. Another source of discrepancy, although less severe than the former, is the absence of hydrodynamic interactions in the LD model as formulated in Eq. (3). Gleim *et al.* have shown for Lennard-Jones liquids that while the β relaxation dynamics depend on the choice of microscopic dynamics used in the simulation, the α relaxation dynamics near the glass transition are independent of that choice [36]. Thus, we do not believe that our choice of ν will affect the alpha relaxation dynamics.

Our results have extended measurements of the long-time dynamic structure factor of concentrated suspensions of alpha crystallin out to a factor of 20 times larger wave vectors than previously studied, and in particular to wave vectors corresponding to the peak in the static structure factor, where LD simulation results are much more reliable. We find relaxation times of order 1000 faster than obtained by DLS, which is consistent with the large q values and the predictions of LD. We also find a decay consistent with LD simulations and a dependence on reduced volume fraction that is consistent with mode coupling theory. When all three complementary techniques (DLS, XPCS, and NSE) are combined they cover wave vectors from 10^7 to 10^9 m^{-1} and time scales from 10^{-7} to 10^2 s. NSE shows good agreement with short-time large q data and theoretical models [37], and XPCS shows good agreement between long-time large q data and LD simulations [10]. DLS covers both short and long time scales and shows agreement with both short- time and long-time theory at small q. The combined agreement lends support to the hard-sphere colloid model as a good description of concentrated suspensions of alpha crystallin.

The good agreement with hard-sphere colloid LD simulations indicates that the technical difficulties associated with radiation damage, fast relaxation times, and extremely small signal-to-noise ratios can be overcome. With the opening and planning of x-ray sources which promise orders of magnitude increases in coherent flux and with the advent of detectors

with submillisecond readout times of megapixel arrays, future experiments on protein dynamics will have the ability to measure faster dynamics with better signal to noise and from lower scattering cross-section materials. These results indicate that XPCS has the potential to become a valuable tool for characterizing protein dynamics in macromolecularly crowded environments. In particular, it is becoming clear that through a combination of different techniques such as DLS, XPCS, and NSE it is now possible to access the dynamics of proteins over a wide range of length scales and time scales providing a much more complete picture of their motion in crowded conditions and a stringent test of theoretical models of their dynamics.

We would like to thank J. DeBartolo, C. DeCaro, and J. Berry for their contributions to this project; in particular, helping to develop techniques to characterize and mitigate radiation damage effects. We would also like to thank Raymond Ziegler for technical support. Research reported in this publication was supported by the National Eye Institute of the National Institutes of Health under Award No. R15EY018249. The content is solely the responsibility of the authors and does not necessarily reflect the official views of the National Institutes of Health. This research used resources of the Advanced Photon Source, a US Department of Energy (DOE) Office of Science User Facility operated for the DOE Office of Science by Argonne National Laboratory under Contract No. DE-AC02-06CH11357. UFXC32k detector development was supported by the National Center for Research and Development, Poland PBS1/A3/12/2012 in the years 2012–2016 and by the National Science Center, Poland, under Contract No. UMO-2016/21/B/ST7/02228.

[1] W. van Megen, T. C. Mortensen, S. R. Williams, and J. Müller, Phys. Rev. E **58**, 6073 (1998).
[2] A. Robert, J. Wagner, W. Härtl, T. Autenrieth, and G. Grübel, Eur. Phys. J. E **25**, 77 (2008).
[3] P. N. Pusey, in *Liquids Freezing and the Glass Transition*, edited by J. P. Hansen, D. Levesque, and J. Zinn (Elsevier, Amsterdam, 1991) Book section10, pp. 763–942.
[4] G. L. Hunter and E. R. Weeks, Rep. Prog. Phys. **75**, 066501 (2012).
[5] J. A. Dix and A. S. Verkman, Ann. Rev. Biophys. **37**, 247 (2008).
[6] A. Giannopoulou, A. J. Aletras, N. Pharmakakis, G. N. Papatheodorou, and S. N. Yannopoulos, J. Chem. Phys. **127**, 205101 (2007).
[7] H. Bloemendal, W. de Jong, R. Jaenicke, N. H. Lubsen, C. Slingsby, and A. Tardieu, Prog. Biophys. Mol. Biol. **86**, 407 (2004).
[8] G. Grübel, A. Madsen, and A. Robert, in *Soft-Matter Characterization*, edited by R. Borsali and R. Pecora (Springer, Heidelberg, 2008), pp. 953–995 .
[9] M. Sutton, C. R. Phys. **9**, 657 (2008).
[10] G. Foffi, G. Savin, S. Bucciarelli, N. Dorsaz, G. M. Thurston, A. Stradner, and P. Schurtenberger, Proc. Natl. Acad. Sci. USA **111**, 16748 (2014).
[11] W. Götze and L. Sjögren, Phys. Rev. A **43**, 5442 (1991).
[12] S. Bucciarelli, J. S. Myung, B. Farago, S. Das, G. A. Vliegenthart, O. Holderer, R. G. Winkler, P. Schurtenberger, G. Gompper, and A. Stradner, Sci. Adv. **2**, e1601432 (2016).
[13] W. Götze, *Complex Dynamics of Glass-Forming Liquids: A Mode-Coupling Theory*, International Series of Monographs on Physics (Oxford University Press, Oxford, 2008).
[14] G. Thurston, J. Chem. Phys. **124**, 134909 (2006).
[15] J. Thomson and R. Augusteyn, Exp. Eye Res. **37**, 367 (1983).
[16] C. DeCaro, V. N. Karunaratne, S. Bera, L. B. Lurio, A. R. Sandy, S. Narayanan, M. Sutton, J. Winans, K. Duffin, J. Lehuta, and N. Karonis, J. Synchrotron Radiat. **20**, 332 (2013).
[17] Q. Zhang, E. M. Dufresne, P. Grybos, P. Kmon, P. Maj, S. Narayanan, G. W. Deptuch, R. Szczygiel, and A. Sandy, J. Synchrotron Radiat. **23**, 679 (2016).
[18] P. Grybos, P. Kmon, P. Maj, and R. Szczygiel, IEEE Trans. Nucl. Sci. **63**, 1155 (2016).
[19] S. Kuwamoto, S. Akiyama, and T. Fujisawa, J. Synchrotron Radiat. **11**, 462 (2004).
[20] P. Vodnala, N. Karunaratne, S. Bera, L. Lurio, G. M. Thurston, N. Karonis, J. Winans, A. Sandy, S. Narayanan, L. Yasui, E. Gaillard, and K. Karumanchi, in *Radiation Damage Limits to XPCS Studies of Protein Dynamics*, edited by Q. Shen and C. Nelson, AIP Conf. Proc. No. 1741 (AIP, Melville, NY, 2016).
[21] A. Vrij, J. Chem. Phys. **71**, 3267 (1979).
[22] W. L. Griffith, R. Triolo, and A. L. Compere, Phys. Rev. A **35**, 2200 (1987).
[23] R. J. Siezen, J. G. Bindels, and H. J. Hoenders, Eur. J. Biochem. **91**, 387 (1978).
[24] A. Tardieu, D. Laporte, P. Licinio, B. Krop, and M. Delaye, J. Mol. Biol. **192**, 711 (1986).
[25] J. Horwitz, Exp. Eye Res. **88**, 190 (2009).
[26] J. A. Carver, J. A. Aquilina, R. J. Truscott, and G. B. Ralston, FEBS Lett. **311**, 143 (1992).
[27] T. M. Treweek, A. Rekas, M. J. Walker, and J. A. Carver, Exp. Eye Res. **91**, 691 (2010).
[28] J. A. Carver, A. B. Grosas, H. Ecroyd, and R. A. Quinlan, Cell Stress & Chaperones **22**, 627 (2017).
[29] K. Schätzel, Quantum Opt. **2**, 287 (1990).
[30] See Supplemental Material at http://link.aps.org/supplemental/10.1103/PhysRevE.97.020601 for additional figures and tables.
[31] M. P. Allen and D. J. Tildesley, *Computer Simulation of Liquids* (Clarendon, New York, 1989).
[32] S. Plimpton, J. Comput. Phys. **117**, 1 (1995).
[33] F. Weysser, A. M. Puertas, M. Fuchs, and Th. Voigtmann, Phys. Rev. E **82**, 011504 (2010).
[34] E. Lange, J. B. Caballero, A. M. Puertas, and M. Fuchs, J. Chem. Phys. **130**, 174903 (2009).
[35] J. T. Padding and A. A. Louis, Phys. Rev. E **74**, 031402 (2006).
[36] T. Gleim, W. Kob, and K. Binder, Phys. Rev. Lett. **81**, 4404 (1998).
[37] A. J. Banchio and G. Nagele, J. Chem. Phys. **128** 104903 (2008).